Auto-focus for Under-sampled Synthetic Aperture Radar

Shaun I. Kelly, Mehrdad Yaghoobi, and Mike E. Davies
Institute for Digital Communications (IDCoM),
University of Edinburgh, UK, EH9 3JL

***Abstract*—We investigate the effects of phase errors on under-sampled synthetic aperture radar (SAR) systems. We show that the standard methods of auto-focus, which are used as a post-processing step, are typically not suitable. Instead of applying auto-focus as a post-processor we propose using a stable algorithm, which is based on algorithms from the dictionary learning literature, that corrects phase errors during the reconstruction and is found empirically to recover sparse SAR images.**

I. Introduction

There are a number of non-standard synthetic aperture radar (SAR) systems, where, without further information, the problem of reconstructing a SAR image from the acquired data is ill-posed. Two such systems are multifunction and ultra wide band (UWB) SAR. In a multifunction SAR system, the radar antenna is used for multiple tasks which causes interruptions in the uniform acquisition of SAR data along the synthetic aperture [1]. In the case of UWB SAR, the transmitted signal spectrum is broad and hence contains sub-bands that are in use by other communications systems or in which transmission is not allowed. To avoid interference, notching filters are commonly introduced into the transmitter and receiver to avoid using these sub-bands [2]. In both these scenarios we have incomplete SAR data and hence without further information, the image reconstruction problem is ill-posed. In order to make the problem well-posed, an appealing idea is to apply the tools and theory of compressed sensing (CS) and sparse approximation.

The theoretical results of CS are based on exact knowledge of the linear acquisition system, however, in practical situations, such a system cannot be known perfectly. This is the case in SAR where the received phase histories contain phase errors due to imperfect system modelling. Traditional SAR systems overcome these errors by post-processing the reconstructed image, a method which may not be compatible with under-sampled SAR.

The paper is organised as follows: in Section II we provide a model of the SAR acquisition system with phase errors. We then describe in Section III how classical methods can fit into the CS framework and their possible short comings. Inherent ambiguities in the under-sampled phase error problem are analysed in Section IV. A practical recovery algorithm for under-sampled SAR with phase errors is proposed in Section V. We then finish with some experimental results in Section VI to demonstrate the effectiveness of the proposed algorithm.

II. SAR Phase Error Model

SAR systems which use dechirp-on-receive must estimate the round trip propagation delay to the scene centre at each position along the aperture. Errors in this estimate, which can be due to a non-idealised propagation medium or inaccuracies in the inertial navigation system, introduce unknown phase errors into the acquired data [3]. If not corrected, phase errors can degrade and produce distortions in the reconstructed image.

Adding a delay error τ_e at each aperture position produces the following SAR system model,

$$y_{kl} = \mathrm{e}^{j\phi_{kl}} \sum_{m=1}^{M}\sum_{n=1}^{N} x_{mn} \exp\left\{-j(\frac{2u_{mnk}}{c} - \tau_0)\left(\omega_0 + 2\alpha\left(lT_s - \tau_0\right)\right)\right\}, \tag{1}$$

where, $\boldsymbol{Y} = \{y_{kl}\} \in \mathbb{C}^{M'\times N'}$ are the phase histories, $\boldsymbol{X} = \{x_{mn}\} \in \mathbb{C}^{M\times N}$ are the scene reflectivities, $\{\phi_{kl}\} = (\omega_0\tau_{\mathrm{e}_k} - \alpha\tau_{\mathrm{e}_k}^2) + 2\alpha\tau_{\mathrm{e}_k}(lT_s - \tau_0) \in \mathbb{C}^{M'\times N'}$ are the phase errors which result from the delay errors, $\{u_{mnk}\} \in \mathbb{R}^{M\times N\times M'}$ are the distances between each element in the scene and each aperture position, c is the speed of light in a vacuum, τ_0 is the true propagation delay to the scene centre, T_s is the range sampling period, 2α is the chirp rate and ω_0 is the carrier frequency. If we neglect the effects of the linear phase term, which is a valid approximation for narrow bandwidth systems, the discrete SAR observation model with phase errors becomes:

$$\boldsymbol{Y} = \operatorname{diag}\left\{\mathrm{e}^{j\boldsymbol{\phi}}\right\} h\left(\boldsymbol{X}\right), \tag{2}$$

where $h : \mathbb{C}^{M\times N} \to \mathbb{C}^{M'\times N'}$ is a linear map that models the ideal SAR observation model which is the summation in (1) and

$$\phi_k = \omega_0\tau_{\mathrm{e}_k} - \alpha\tau_{\mathrm{e}_k}^2 \tag{3}$$

are the constant phase errors.

Clearly, without further assumptions, the problem of recovering $\boldsymbol{\phi}$ and $\boldsymbol{X}$ from $\boldsymbol{Y}$ is ill-posed if $M' = M$ and $N' = N$, since there are only MN equations and $M(N+1)$ unknowns.

III. Classical Auto-focus

Classical auto-focus methods such as the phase gradient auto-focus (PGA) algorithm [4] make a far-field and small aperture angle approximation in the standard dechirped SAR acquisition system, e.g. see [3]. Under these approximations the system can be modelled as a LHS and RHS matrix multiplication as in

$$\boldsymbol{Y} = \operatorname{diag}\left\{\mathrm{e}^{j\phi}\right\}\boldsymbol{A}\boldsymbol{X}\boldsymbol{B}, \tag{4}$$

where, $a_{mn} = \exp\{-j(2\pi(m-1)(n-1)/M-(m-1)\pi-(n-1)\pi + M\pi/2)\}$ and $b_{mn} = \exp\{-j(2\pi(m-1)(n-1)/N - (m-1)(2\pi\omega_o/2\alpha T-\pi)-(n-1)\pi+N\pi/2-2\omega_o L/c)\}$ are the elements of the cross-range matrix $\boldsymbol{A} \in \mathbb{C}^{M\times M}$ and the range matrix $\boldsymbol{B} \in \mathbb{C}^{N\times N}$ respectively, where, L is the scene radius and T is the chirp period.

Since, $\boldsymbol{A}$ is essentially a Fourier matrix, we can rewrite the observation model in (4) as $\boldsymbol{Y} = \boldsymbol{A}\boldsymbol{\Psi}\boldsymbol{X}\boldsymbol{B}$, where, $\boldsymbol{\Psi}$ is a circulant matrix which can be viewed as a filter in cross-range.

Classical auto-focus algorithms recover $\boldsymbol{\Psi}\boldsymbol{X}$ from $\boldsymbol{Y}$, which is straight forward because $\boldsymbol{A}$ and $\boldsymbol{B}$ are invertible. $\boldsymbol{X}$ is then recovered from the filtered image $\boldsymbol{\Psi}\boldsymbol{X}$, by assuming additional constraints on $\boldsymbol{\Psi}$ and $\boldsymbol{X}$.

When $\boldsymbol{Y}$ is under-sampled in cross-range the observation model will be:

$$\boldsymbol{Y'} = \boldsymbol{A'}\boldsymbol{\Psi}\boldsymbol{X}\boldsymbol{B}, \tag{5}$$

where, $\boldsymbol{A'} \in \mathbb{C}^{M'\times M}$ is a $M' < M$ row subset of $\boldsymbol{A}$. With this model, unlike in the fully-sampled situation, $\boldsymbol{A'}$is not invertible. However, CS results can be used analyse the expected reconstruction quality of $\boldsymbol{\Psi}\boldsymbol{X}$ when it is reconstructed by solving a non-linear reconstruction algorithm.

If the under-sampling in Eq.(5) is random, a sufficient order for the number of cross-range samples required for stable reconstruction is $\mathcal{O}(K\log^4(M))$, for, $K = K_{\boldsymbol{\psi_m}}K_{\boldsymbol{X}}$, where, $K_{\boldsymbol{\psi_m}}$ and $K_{\boldsymbol{X}}$ are the maximum required number of non-zero elements needed to accurately approximate the rows of $\boldsymbol{\Psi}$ and the columns of the true image $\boldsymbol{X}$, respectively. The reconstruction is stable in the sense that the columns of the recover image $\widetilde{\boldsymbol{\Psi}\boldsymbol{X}}$ satisfies:

$$\|\tilde{\boldsymbol{x}} - \boldsymbol{x}\|_2 \leq C_{1,K}\sigma + C_{2,K}\frac{\|\boldsymbol{x}-\boldsymbol{x}_K\|_1}{\sqrt{K}}\ [5], \tag{6}$$

in words, the solution will be bounded by something that is proportional to the noise energy σ and the error associated with the best K-term approximation of $\boldsymbol{x}$.

If the under-sampling in Eq.(5) is random, a sufficient order for the number of range samples required for stable reconstruction is $\mathcal{O}(K\log^4(N))$, for, $K = K_{\boldsymbol{\Psi X}}$, where, $K_{\boldsymbol{\Psi X}}$ is the maximum required number of non-zero elements needed to accurately approximate the rows of $\boldsymbol{\Psi}\boldsymbol{X}$. The reconstruction is stable in the sense that the rows of the recover image $\widetilde{\boldsymbol{\Psi}\boldsymbol{X}}$ satisfy Eq. (6).

It is clear that the number of samples required for a stable reconstruction scales with $K_{\boldsymbol{\psi_m}}$ and thus the introduction of phase errors increases the number of samples required for stable reconstruction. For this reason, in most cases, post-processing autofocus methods are unsuitable for under-sampled SAR.

IV. Uniqueness

It is well known that there are inherit ambiguities in the auto-focus problem which prevent the problem having a unique solution. The formulation in (4) is known to be ambiguous to constant and linear phase errors [3].

The uniqueness of the auto-focus problem is dependent on the observation model h and the signal model of the scene X. A necessary condition to guarantee uniqueness of the problem is as follows:

$$h\left(\tilde{\boldsymbol{X}}\right) = \operatorname{diag}\{\boldsymbol{d}\}h\left(\boldsymbol{X}\right) \iff \tilde{\boldsymbol{X}} = \beta\boldsymbol{X}, \tag{7}$$

$$\forall(\tilde{\boldsymbol{X}}, \boldsymbol{X}, \boldsymbol{d}) \in \left\{\tilde{\boldsymbol{X}} \in \mathcal{X}, \boldsymbol{X} \in \mathcal{X}, \boldsymbol{d} \in \mathcal{D}\right\},$$

where,

$$\mathcal{X} = \left\{\boldsymbol{X} \in \mathbb{C}^{M\times N} : \|\boldsymbol{X}\|_0 \leq K\right\},$$

i.e. we know the scene has at most K scatters, and

$$\mathcal{D} = \left\{\boldsymbol{d} \in \mathbb{C}^{M'} : |d_m| = 1\right\}$$

is the set of all possible phase errors.

If 7 is satisfied then the problem is unique up to a scalar $\beta \in \{\beta \in \mathbb{C} : |\beta| = 1\}$ multiplication of the true $\boldsymbol{X}$, i.e. $\tilde{\boldsymbol{X}} = \beta\boldsymbol{X}$, and the solutions are given by the following program:

$$\begin{aligned} \underset{\boldsymbol{X},\boldsymbol{d}\in\mathcal{D}}{\text{minimise}} \quad & \|\boldsymbol{X}\|_0 \\ \text{subject to} \quad & \operatorname{diag}\{\boldsymbol{d}\}\boldsymbol{Y} = h\left(\boldsymbol{X}\right) \end{aligned} \tag{8}$$

where, $\|.\|_0$ measures the number of non-zeros matrix elements.

V. Robust Convex Relaxation

With the goal of designing an algorithm that is able to be solved in polynomial time and which is also robust to noise, the non-convex function $\|\boldsymbol{X}\|_0$ in (8) can be replaced with its closest convex function $\|\boldsymbol{X}\|_1$ and the equality constraint can be replaced with an inequality constraint that accommodates noise, i.e.

$$\begin{aligned} \underset{\boldsymbol{X},\boldsymbol{d}}{\text{minimise}} \quad & \|\boldsymbol{X}\|_1 \\ \text{subject to} \quad & \|\operatorname{diag}\{\boldsymbol{d}\}\boldsymbol{Y} - h(\boldsymbol{X})\|_F \leq \sigma \\ & d_m^* d_m = 1,\ m = 1,\ldots,M. \end{aligned} \tag{9}$$

Even though our objective function is now convex, (9) is still non-convex because the equality constraint is not linear and therefore does not define a convex feasible set.

A convenient formulation is to exchange to the inequality constraint and the objective to form:

$$\begin{aligned} \underset{\boldsymbol{X},\boldsymbol{d}}{\text{minimise}} \quad & \left\|\text{diag}\left\{\boldsymbol{d}\right\}\boldsymbol{Y}-h(\boldsymbol{X})\right\|_F^2 \\ \text{subject to} \quad & \left\|\boldsymbol{X}\right\|_1 \leq \tau \\ & d_m^* d_m = 1,\ m=1,\ldots,M, \end{aligned} \tag{10}$$

where, there is a one-to-one map, $\gamma : \sigma \rightarrow \tau$ if $0 \leq \sigma \leq \left\|\boldsymbol{Y}\right\|_F$. The problem is still non-convex, however importantly, in each set of variables $\boldsymbol{X}$ and $\boldsymbol{d}$ –with the other fixed– we have a unique solution. This observation allows us to use a block relaxation type method which has been found to be effective in dictionary learning [6].

A. Majorisation Minimisation Method

Consider (10) when $\boldsymbol{d}$ is fixed, i.e.

$$\begin{aligned} \underset{\boldsymbol{X}}{\text{minimise}} \quad & f(\boldsymbol{X},\boldsymbol{d}), \\ \text{subject to} \quad & \left\|\boldsymbol{X}\right\|_1 \leq \tau \end{aligned} \tag{11}$$

where,

$$f(\boldsymbol{X},\boldsymbol{d}) = \left\|\text{diag}\left\{\boldsymbol{d}\right\}\boldsymbol{Y}-h(\boldsymbol{X})\right\|_F^2. \tag{12}$$

A method used for solving (11) is a technique known as "majorisation minimisation". This technique replaces the objective function with a surrogate function which is much easier to solve. We can define our surrogate function as,

$$\begin{aligned} g(\boldsymbol{X},\boldsymbol{X}^\ddagger,\boldsymbol{d}) = & \left\|\text{diag}\left\{\boldsymbol{d}\right\}\boldsymbol{Y}-h(\boldsymbol{X})\right\|_F^2 - \\ & \left\|h\left(\boldsymbol{X}-\boldsymbol{X}^\ddagger\right)\right\|_F^2 + \\ & L\left\|\boldsymbol{X}-\boldsymbol{X}^\ddagger\right\|_F^2. \end{aligned} \tag{13}$$

Replacing the objective function with the surrogate function, (11) becomes

$$\begin{aligned} \underset{\boldsymbol{X},\boldsymbol{X}^\ddagger}{\text{minimise}} \quad & g\left(\boldsymbol{X},\boldsymbol{X}^\ddagger,\boldsymbol{d}\right) \\ \text{subject to} \quad & \left\|\boldsymbol{X}\right\|_1 \leq \tau, \end{aligned} \tag{14}$$

which is a minimisation based on $\boldsymbol{X}$ and a surrogate parameter vector $\boldsymbol{X}^\ddagger$. In this program, if $\boldsymbol{X}$ is fixed, the minimum of (14) occurs at $\boldsymbol{X}^\ddagger = \boldsymbol{X}$ and if $\boldsymbol{X}^\ddagger$ is fixed the minimum occurs at

$$\begin{aligned} \underset{\boldsymbol{X}}{\text{minimise}} \quad & \left\|\boldsymbol{X}-\boldsymbol{C}\right\|_F \\ \text{subject to} \quad & \left\|\boldsymbol{X}\right\|_1 \leq \tau \end{aligned} \tag{15}$$

where, $\boldsymbol{C} = \boldsymbol{X}^\ddagger + \frac{1}{L}h^{\text{H}}(\text{diag}\left\{\boldsymbol{d}\right\}\boldsymbol{Y} - h(\boldsymbol{X}^\ddagger))$. Which is the projection of $\boldsymbol{C}$ onto an ℓ_1 ball with a radius of τ. There are efficient methods to exactly compute this projection [7].

By minimising (14) based on either $\boldsymbol{X}^\ddagger$ and $\boldsymbol{X}$ in an alternating fashion, $\boldsymbol{X}^\ddagger$ and $\boldsymbol{X}$ will converge to the solution of (11) so long as $L \geq \left\|h\right\|^2$ [8], where, $\left\|h\right\| = \sup\left\{\left\|h(\boldsymbol{X})\right\|_F : \boldsymbol{X} \in \mathbb{C}^{M\times N} \text{ with } \left\|\boldsymbol{X}\right\|_F = 1\right\}$ is the operator norm of h. In practice a feasible L can determined using a backtracking line-searching.

B. Phase Minimisation

Consider (10) when $\boldsymbol{X}$ is fixed, which (ignoring constant terms) is given by:

$$\begin{aligned} \underset{\boldsymbol{d}}{\text{minimise}} \quad & \text{tr}\left\{-2\,\text{Re}\left\{\text{diag}\left\{\boldsymbol{d}^{\text{H}}\right\}h(\boldsymbol{X})\boldsymbol{Y}^{\text{H}}\right\}\right\} \\ \text{subject to} \quad & d_m^* d_m = 1,\ m=1,\ldots,M. \end{aligned} \tag{16}$$

The unique solution of which is,

$$\boldsymbol{d} = e^{j\angle\text{diag}\left\{h(\boldsymbol{X})\boldsymbol{Y}^{\text{H}}\right\}}. \tag{17}$$

C. Block Relaxation Auto-focus

If we alternate between solving (11) and (16) in an alternating fashion this can be seen as a block relaxation of (10) the pseudo code of which is as follows:

Algorithm 1 $\mathcal{A}(\boldsymbol{X},\boldsymbol{d})$

Output: $\boldsymbol{X},\boldsymbol{d}$
  repeat
    $\boldsymbol{X}^\ddagger \leftarrow \boldsymbol{X}$
    $\boldsymbol{X} \leftarrow \mathcal{C}(\boldsymbol{X},\boldsymbol{d})$
    $\boldsymbol{d}^\ddagger \leftarrow \boldsymbol{d}$
    $\boldsymbol{d} \leftarrow e^{j\angle\text{diag}\left\{h(\boldsymbol{X})\boldsymbol{Y}^{\text{H}}\right\}}$
  until $\left\|\boldsymbol{X}-\boldsymbol{X}^\ddagger\right\|_F <$ threshold $\wedge$ $\left\|\boldsymbol{d}-\boldsymbol{d}^\ddagger\right\|_F <$ threshold

Where, $\mathcal{C}$ solves (11). The approaches used in [9] and [10] are of this form. This type of method is known to be stable assuming we can solve $\mathcal{C}$, i.e. we exactly solve (11) at each iteration. In practical systems where only an approximate solution at each iteration can be obtained, no stability analysis exists.

Another way to create a block relaxation is to consider the problem with three blocks of parameters, i.e.

$$\begin{aligned} \underset{\boldsymbol{X},\boldsymbol{X}^\ddagger,\boldsymbol{d}}{\text{minimise}} \quad & g\left(\boldsymbol{X},\boldsymbol{X}^\ddagger,\boldsymbol{d}\right) \\ \text{subject to} \quad & \left\|\boldsymbol{X}\right\|_1 \leq \tau \\ & d_m^* d_m = 1,\ m=1,\ldots,M, \end{aligned} \tag{18}$$

As long as (18) is minimised by varying $\boldsymbol{X}$ followed by $\boldsymbol{X}^\ddagger$ the solution for each sub-problem is easily commutable and the complete algorithm is known to be stable and guaranteed to converge to a accumulation point or a connected set of accumulation points [6]. The pseudo code for this algorithm, when phase minimisation occurs at each iteration, is as follows:

Where, $\mathcal{P}_\tau(\boldsymbol{C})$ projects $\boldsymbol{C}$ onto an ℓ_1 ball with a radius of τ. It is interesting to note that this algorithm can be seen as a generalisation of Algorithm 1.

VI. Experimental Results

In these experiments we investigate the reconstruction performance of Algorithm 2 using under-sampled phase histories that contain phase errors.

Algorithm 2 $\mathcal{B}(\boldsymbol{X}, \boldsymbol{d})$

Initialise: $L \geq \|h\|_F^2$
Output: $\boldsymbol{X}, \boldsymbol{d}$
  repeat
    $\boldsymbol{X}^\ddagger \leftarrow \boldsymbol{X}$
    $\boldsymbol{C} \leftarrow \boldsymbol{X}^\ddagger + \frac{1}{L} h^{\mathrm{H}} \left(\mathrm{diag}\left\{\boldsymbol{d}\right\} \boldsymbol{Y} - h\left(\boldsymbol{X}^\ddagger\right)\right)$
    $\boldsymbol{X} \leftarrow \mathcal{P}_\tau(\boldsymbol{C})$
    $\boldsymbol{d}^\ddagger \leftarrow \boldsymbol{d}$
    $\boldsymbol{d} \leftarrow e^{j \angle \mathrm{diag}\left\{h(\boldsymbol{X}) \boldsymbol{Y}^{\mathrm{H}}\right\}}$
  until $\left\| \boldsymbol{X} - \boldsymbol{X}^\ddagger \right\|_F <$ threshold $\wedge$ $\left\| \boldsymbol{d} - \boldsymbol{d}^\ddagger \right\|_F <$ threshold

A. Synthetic Point-targets

In the first experiment we consider random under-sampling of the synthetic aperture. In order to compare classical techniques with Algorithm 2, we consider the model used in classical auto-focus method techniques, (4). The scene consists of a small number of constant amplitude point targets randomly placed in the scene with additive Gaussian clutter. Quadratic phase errors of the form, $\phi_m = \gamma((m-1)/M)^2$, were added to simulate platform velocity measurement errors. The parameters for the synthetic model are in Table. I.

TABLE I
SAR SYSTEM PARAMETERS FOR SYNTHETIC EXPERIMENTS

parameter	value
carrier frequency (ω_o)	$2\pi \times 10 \times 10^9$ rad/s
chirp bandwidth ($2\alpha T$)	$2\pi \times 150 \times 10^6$ rad/s
scene radius (L)	50 m
number of targets	20
target to clutter ratio	50 dB

In order to assess the image reconstruction performance of the two methods we define an image quality metric. Since the auto-focus problem is ambiguous to scalar multiplication by $\beta \in \{\beta \in \mathbb{C} : |\beta| = 1\}$ and cyclic permutation, we define a metric that is immune to these ambiguities. We will refer to this metric as relative SNR and define it as:

$$\max_{\beta, n} \left\{ 10 \log_{10} \left(\frac{\left\| \tilde{\boldsymbol{X}} \right\|_F^2}{\left\| \tilde{\boldsymbol{X}} - \beta \boldsymbol{P}^n \boldsymbol{X} \right\|_F^2} \right) \right\},$$

where, $n \in \mathbb{Z}$ and

$$P = \begin{bmatrix} 0 & 0 & \dots & 0 & 1 \\ 1 & 0 & \dots & 0 & 0 \\ 0 & \ddots & \ddots & \vdots & \vdots \\ \vdots & \ddots & \ddots & 0 & 0 \\ 0 & \dots & 0 & 1 & 0 \end{bmatrix}.$$

Fig. 2 shows the reconstruction performance of oracle classical auto-focus and Algorithm 2 with three different quadratic phase errors. We refer to it as oracle classical auto-focus because we use a ℓ_1-norm spectral projected gradient (SPG) method [8] to recover the filtered image and then correct it to recover the image using oracle knowledge of the phase errors. To provide an empirical upper-bound, we also show the reconstruction performance that can be achieved with oracle knowledge of the phase errors and also the locations of the targets, we refer to this as the oracle reconstruction. The magnitude of the corresponding filters for each of the phase errors, the rows of Ψ, are shown in Fig. 1. As predicted in Section III, as the value of $K_{\boldsymbol{\psi}_m}$ increases, corresponding to an increase in γ, the performance of classical auto-focus techniques decreases, while the performance of Algorithm 2 is consistent.

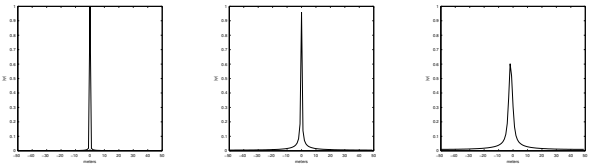

(a) (b) (c)

Fig. 1. Phase error induced filters: the rows of Ψ, with different γ. (a) $\gamma = 0.1$ (b) $\gamma = 1$ (b) $\gamma = 10$

B. GOTCHA Data Set

In the second experiment we consider random under-sampling of the publicly available Gotcha data set [11] in the range direction which simulates transmitter and receiver notch filtering. To realistically model phase errors we add errors to the supplied aperture position data such that errors in the distance to the scene centre measurements, which are used in observational model, are normally distributed with a variance of 6.8×10^{-6} meters. In this experiment, the more general –non Fourier– model (4) is used, where we compute the observation model and its adjoint using the fast (re/back)-projection algorithms from [10]. A classical auto-focus method was not used in this experiment because even with only two degrees of the Gotcha data set, the observation model is not well-approximated by (4). Fig. 3(a) shows the reconstructed image using a ℓ_1-norm SPG method. Fig. 3(b) shows the reconstructed image using Algorithm 2. The reduction in side lobes in Fig. 3(b) clearly demonstrates that Algorithm 2 is effectively reconstructing the bright targets and correcting the phase errors in a realistic under-sampled SAR problem.

VII. Conclusion

We have investigated the effects of phase errors on a under-sampled SAR system. We have demonstrated that traditional SAR auto-focus methods, that are a post-processing procedure, are in most cases unsuitable when there is under-sampling. We have also proposed and demonstrated empirically a stable algorithm that can correct phase errors and recover a sparse SAR image from an under-sampled phase history.

Acknowledgment

This work was supported in part by: EPSRC grants [EP/F039697/1, EP/H012370/1], the MOD University Defence

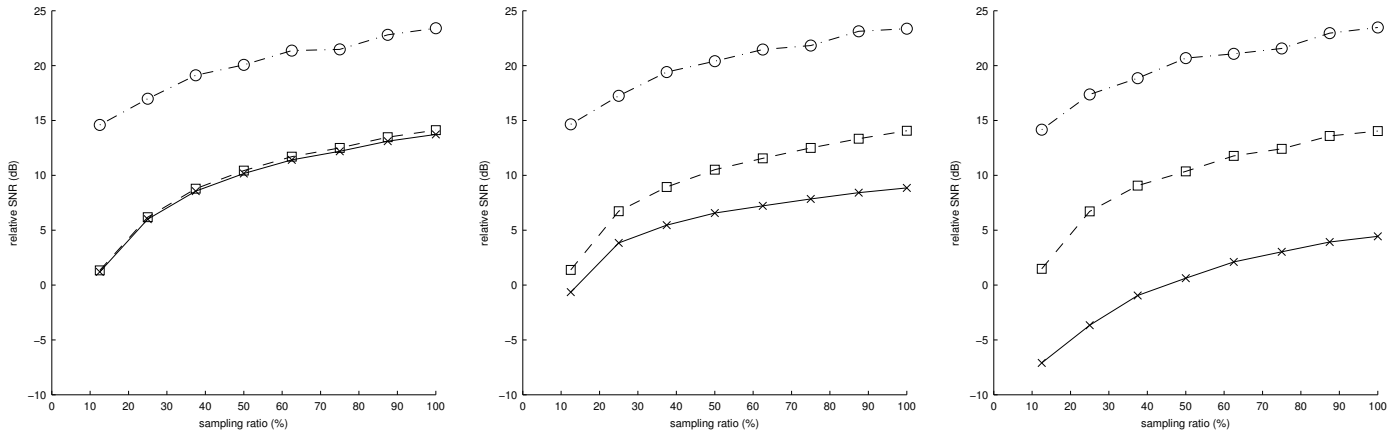

(a) (b) (c)

Fig. 2. Reconstruction performance versus under-sampling ratio: '$\circ$', oracle reconstruction, '$\square$' Algorithm 2 and '$\times$' oracle classical auto-focus (a) $\gamma = 0.1$ (b) $\gamma = 1$ (b) $\gamma = 10$

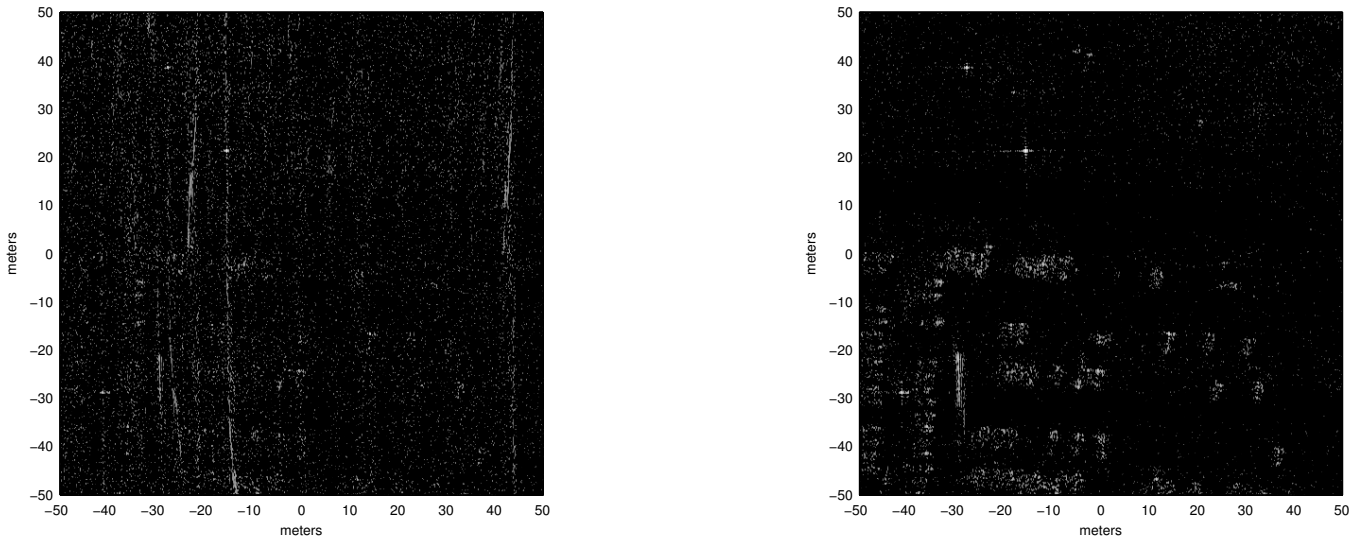

(a) (b)

Fig. 3. Reconstructions from 2° of the Gotcha data set with under-sampling in range and phase errors. (a) reconstructed image using an ℓ_1-norm SPG method (b) reconstructed image using Algorithm 2

Research Centre on Signal Processing and the European Commission through the SMALL project under FET-Open, grant number 225913.

REFERENCES

[1] J. Salzman, D. Akamine, R. Lefevre, and J. Kirk, J.C., "Interrupted synthetic aperture radar (SAR)," in *Proc. of IEEE Radar Conf.*, May 2001, pp. 117–122.

[2] M. Davis, *Foliage penetration radar*, 1st ed. SciTech Publishing, 2011.

[3] C. Jakowatz Jr, D. Wahl, P. Eichel, D. Ghiglia, and P. Thompson, *Spotlight-mode synthetic aperture radar: a signal processing approach*, 4th ed. Kluwer Academic Publishers, 1999.

[4] D. Wahl, P. Eichel, D. Ghiglia, and C. Jakowatz Jr, "Phase gradient autofocus-a robust tool for high resolution SAR phase correction," *IEEE Trans. Aerosp. Electron. Syst.*, vol. 30, no. 3, pp. 827–835, Jul. 1994.

[5] E. Candes, J. Romberg, and T. Tao, "Stable signal recovery from incomplete and inaccurate measurements," *Commun. Pure Appl. Math.*, vol. 59, no. 8, pp. 1207–1223, 2006.

[6] M. Yaghoobi, T. Blumensath, and M. Davies, "Dictionary learning for sparse approximations with the majorization method," *IEEE Trans. Signal Process.*, vol. 57, no. 6, pp. 2178–2191, Jun. 2009.

[7] J. Duchi, S. Shalev-Shwartz, Y. Singer, and T. Chandra, "Efficient projections onto the ℓ_1-ball for learning in high dimensions," in *Proc. of ICML*, 2008, pp. 272–279.

[8] E. Birgin, J. Martínez, and M. Raydan, "Nonmonotone spectral projected gradient methods on convex sets," *SIAM J. Optim.*, vol. 10, no. 4, pp. 1196–1211, 2000.

[9] N. Onhon and M. Cetin, "A sparsity-driven approach for joint SAR imaging and phase error correction," *IEEE Trans. Image Process.*, vol. 21, no. 4, pp. 2075–2088, Apr. 2012.

[10] S. Kelly, G. Rilling, M. Davies, and B. Mulgrew, "Iterative image formation using fast (re/back)-projection for spotlight-mode SAR," in *Proc. of IEEE Radar Conf.*, May 2011, pp. 835–840.

[11] C. Casteel Jr, L. Gorham, M. Minardi, S. Scarborough, K. Naidu, and U. Majumder, "A challenge problem for 2D/3D imaging of targets from a volumetric data set in an urban environment," in *Proc. SPIE*, vol. 6568, Apr. 2007.